Supporting Information

Simultaneous multi-angle AR-XANES for surface-sensitive chemical speciation of gold nanolayers in wall painting replica

Maram Na'es,*[a] Lars Lühl, [a,b] Daniel Grötzsch,[a] Ioanna Mantouvalou, [a,c] Jonas Baumann[d] and Birgit Kanngießer [a]

Institute for Optics and Atomic Physics, Technical University Berlin, Hardenbergstr. 36, 10623 Berlin. E-mail: maram@physik.tu-berlin.de

current address Pfeiffer Vacuum GmbH, Germany.

Helmholtz Zentrum Berlin HZB.

Current address Bruker Nano GmbH, Berlin.

Electronic Supplementary Information (ESI) available: [details of any supplementary information available should be included here]. See DOI: 10.1039/x0xx00000x

Sample Preparation

Since the experimental conservation material was designed based on the study of condition and composition of Nabataean gilded wall paintings and stucco from Petra in Jordan, artificial corrosive environments were designed following elevated factors of main causes of damage existing in Petra's environment[1,2]. Test samples were exposed to a combination of thermal and UV radiation corrosion causes. Starting with heating at 100 °C for 180 minutes followed by 240 minutes exposure to UV 366 nm radiation from a 6 V UV lamp (A.KRÜSS Optronic GmbH, UVT3600) at room temperature. After this treatment, delamination of the gold layer was visually detectable.

The intervention was made by injecting 10 µL of NGG-1b solution at room temperature and pressure in areas under lifted gold leaves. No pre-wetting was used, and multiple gradual applications were performed up to 200 µL maximum. To ensure that a compatible amount of the adhesive gel is used, gentle mechanical repositioning of the leaf was made with the aid of a fine gilding brush (Kremer Pigmente, ID# 85413202) through a layer of Japanese tissue (Kremer Pigmente, ID# 875080).

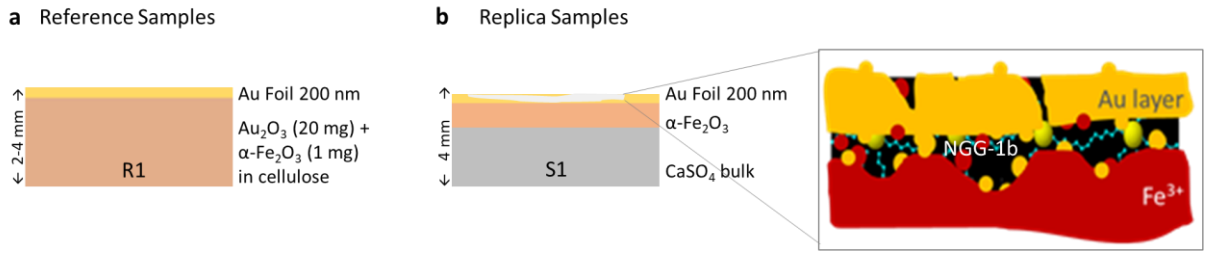

Figure S1: Schematic illustration of layered structure and composition of (a) reference samples and (b) replica samples investigated by AR-XANES analysis. Grey layer at the interface between Au foil and iron-containing layer in (b) is the experimental conservation adhesive NGG-1b. Its location and distribution are visualised to the right.

XANES analysis

Table S1: Scanning settings used for conventional XANES and EXAFS measurements at a 90° geometry between excitation beam and detected fluorescence radiation.

Energy Range (eV)	Step size (eV)	Acquisition time/step (sec.)	# of steps
11800 - 11900	10	4	10
11890 - 11960	0.5	4	140
11959 - 12100	1	4	141
12000 – 12400	10	4	40

Table S2. List of filters available at MySpot Beamline and their properties. In bold are the filters used in our experiments.

Filter #	Material	Thickness (mm)
1	**empty**	**0**
2	Cu	0.2
3	Cu	0.1
4	Cu	0.065
5	Al	4
6	Al	2
7	Al	1
8	**Al**	**0.5**
9	**Al**	**0.2**
10	**Al***	**0.06**
11	Cu	0.034
12	Pt	0.0075
13	Au	0.008
* commercial Al foil		

AR-XANES slit-cap

Sample positioning was automated and controlled using a 5-axis positioning stage with 3 translational and 2 rotational movements. A holder was used to mount single and multiple samples in a precise geometry. Changing samples was facilitated using a microscope mounted between the excitation beam lens and the detector. The experimental hutch is equipped with an air conditioner, and a temperature and humidity sensor positioned in the vicinity of the sample (AT: 18-24 °C ± 1 °C, RH 40-55 % ± 1 %)[3]. All measurements were performed in air.

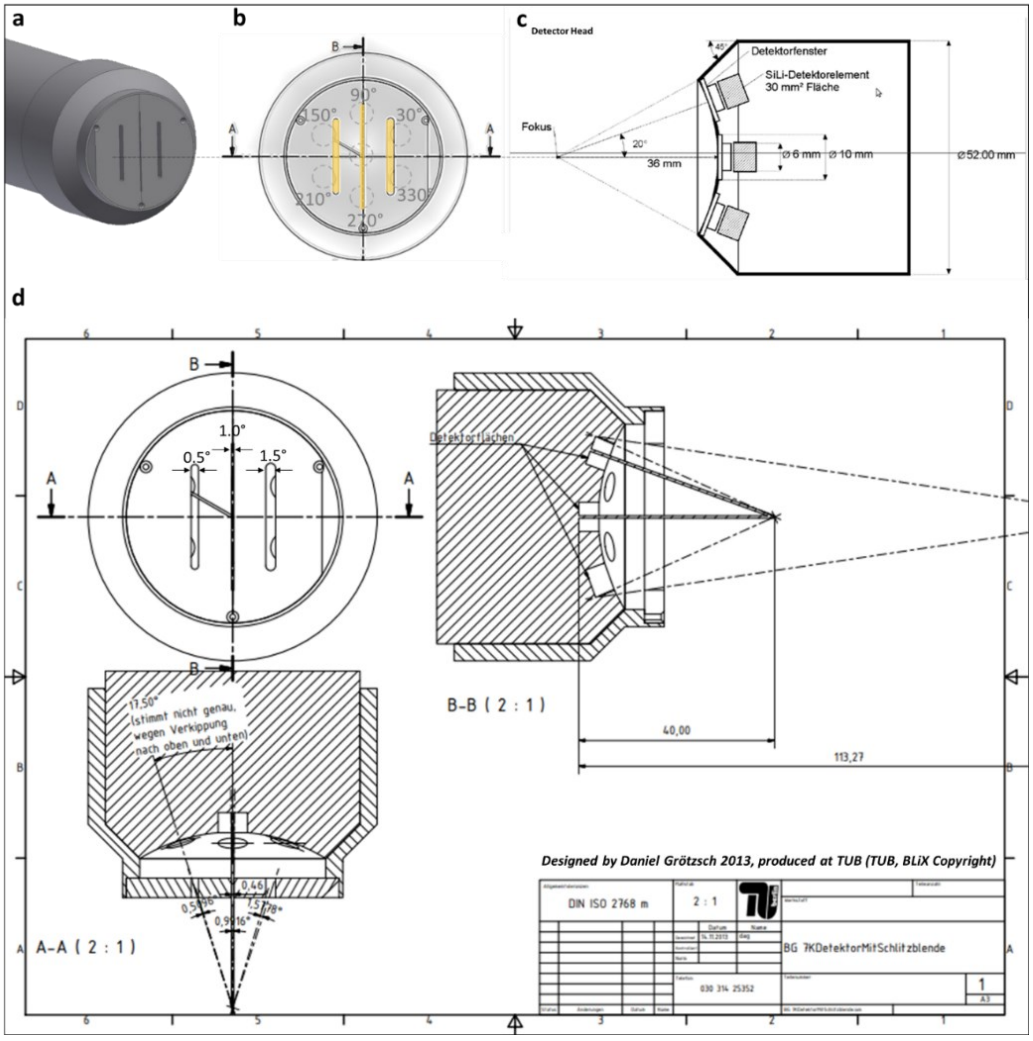

Figure S2: Design sketches of the slit-cap for GE angle-resolved measurements specifically designed and used for this experiment (Copyright ©BLiX, TUB 2013). (a) Slit-cap overview. (b) Geometrical arrangement of the seven element detector windows behind the slit-cap and the three vertical detectors arrays of slits highlighted yellow. (c) Side view of the detector head showing three of the 7-element detector on a semi-sphere arrangement. (d) Slit-cap front view indicating slit widths (top left), vertical side view (top right), and horizontal side view or top view showing beam divergence for each slit (bottom).

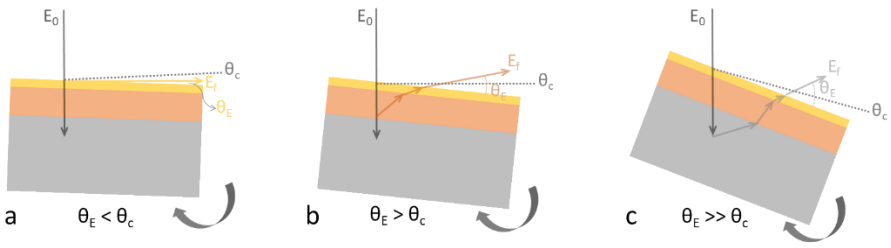

Figure S3: Schematic representation of GE geometry at exit angles (a) less than the critical angle where detected fluorescence is surface sensitive, (b) larger than the critical angle where detected fluorescence originates from deeper probed layers, (c) much larger than the critical angle where much deeper layers can be detected. (E_0: photon energy of excitation radiation, E_f: photon energy of fluorescence radiation, θ_c: critical angle of total reflection, θ_E: exit angle at which E_f is detected).

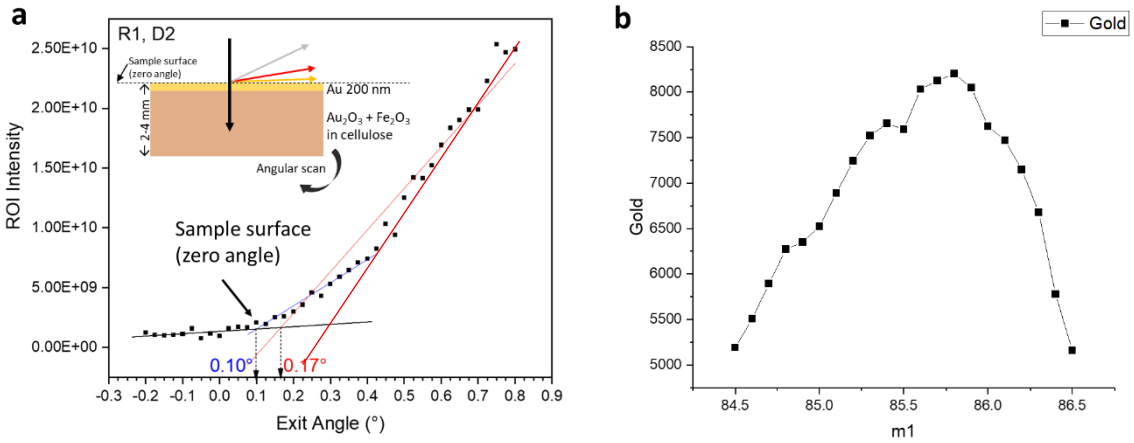

Figure S4: (a) Angular dependence of Au-$L_{\alpha 1}$ fluorescence intensity for reference sample R1 (inset) probed at fixed excitation photon energy (12.1 keV) to determine sample surface (zero angle) with ± 0.1° angular resolution. (b) Signal optimisation at the zero angle position determined by scanning gold intensity along the z-axis perpendicular to sample surface (in depth).

Table S3: Characteristic XANES absorption energies (± 0.5 eV) as measured for gold reference species (S: sharp, sh: shoulder, wk: weak, w: wide)

Characteristic Peak	Au Foil (5 µm)	Au_2S	Au_2O_3	$HAuCl_4.3H_2O$
L_3 Edge (E_0)	11919	11921.3	11918.5	11918
L_3 transition	$2p_{3/2} \rightarrow$ 5d and 6s	$2p_{3/2} \rightarrow$ 5d and 6s	$2p_{3/2} \rightarrow$ 5d	$2p_{3/2} \rightarrow$ 5d
Au Electronic Configuration	[Xe] $4f^{14}$ $5d^{10}$ $6s^1$ $\leftrightarrow$ [Xe] $4f^{14}$ $5d^9$ $6s^2$	[Xe] $4f^{14}$ $5d^{10}$ $6s^0$ $\leftrightarrow$ [Xe] $4f^{14}$ $5d^9$ $6s^1$	[Xe] $4f^{14}$ $5d^8$ $6s^0$ $\leftrightarrow$ [Xe] $4f^{14}$ $5d^6$ $6s^2$	[Xe] $4f^{14}$ $5d^8$ $6s^0$ $\leftrightarrow$ [Xe] $4f^{14}$ $5d^6$ $6s^2$
1st	11924.5 (wk)	11925 (wk)	11922.5 (S)	11921.5 (S)
	11934 (w)	11934 (wk)	11935	11934 (w)
2nd	11948 (S)	11948.5 (w)	11940 (sh)	-
3rd	11970 (S)	11970 (S)	11970 (S)	11970 (w)
4th	12080 (w)	12105 (w)	12128 (w)	12100 (w)

A quantitative comparison of absorption edge energy (E_0) and white line intensity (WL) for reference R1 and replica S1 samples at various angles and detectors was used to describe spectral, hence, chemical differences, those are shown in Figure S5. Two spectral parameters, white line intensity (WL) and absorption edge energy (E_0) were extracted from Au-L_3 AR-XANES spectra and compared with corresponding values of raw NGG-1b and gold standards to find any change in chemical speciation (valency) upon application on the composite structure (*in vivo* assessment). White line intensity (WL) was determined from the maximum value of the AR-XANES rising profile after the edge (white line region). Absorption edge energy (E_0) was determined from the position of dµ/dE maxima of the corresponding AR-XANES spectrum. Energy shift (ΔE_0) of the absorption edge of AR-XANES spectra at various angles was then obtained in reference to raw NGG-1b. This way, spectral features of Au-L_3 AR-XANES at all measured angles from the three sets of detectors arrays could be compared. It is to be noted that uncertainty for E_0 and ΔE_0 is ± 0.5 eV, and ± 0.05 for WL intensity.

From Figure S5a it can be said that absorption edge energies of reference sample R1 at the three detectors for exit angles 20° and below are indicative for irregularities in the sample surface. This is also clear in absorption edge values at surface and near surface layers which variate around E_0 for Au(0). The replica sample S1 shows values between Au(0) and Au(I) species at all exit angles. Though the lower angles (< 10°) representing near surface composition show a decrease in Au(I) features and an increase in Au(0) features as also seen in LCF discussed earlier. The absorption edge energies for R1 at all detectors show almost a steady value that matches Au(0) edge energy. Despite that Au(III) signal is expected to be seen at larger angles of detection since the bottom layer of R1 is composed of Au_2O_3, but it is not seen in edge energy shifts. Regarding S1, the blue energy shift (towards higher E) is observed with an average value of 0.5 eV which is within the experimental uncertainty. But since the shift remains almost constant through the sample depth, it indicates a homogeneous behaviour of NGG-1b at surface and in-depth regardless of interface composition.

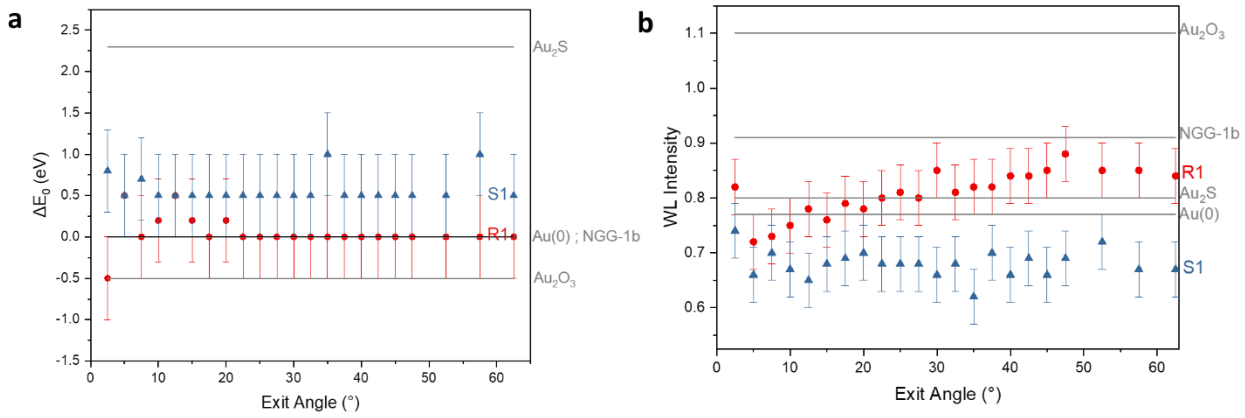

Figure S5: (a) Shift of absorption edge energy ΔE_0 of Au-L_3 AR-XANES spectra, in reference to raw NGG-1b, for reference R1 and replica S1 samples at all detector arrays. (b) White line intensity (WL) of Au-L_3 AR-XANES spectra for R1 and S1 at all angles. Values for gold standards and raw NGG-1b are marked in horizontal grey lines.

Comparing white line intensity (WL) shown in Figure S5b, values for reference sample R1 at all three sets of detectors arrays show an increasing profile that starts below Au(0) intensity and continues gradually above WL intensity of Au_2S with a maxima at 47.5° approaching NGG-1b intensity. It is expectable to have a large impact of Au(0) layer (200 nm thick) above Au_2O_3 bulk seen in high absorption of Au(III) fluorescence signal leaving the surface. This also appears in a damped WL intensity as shown in Figure S5b. On the other hand, the replica sample measured at the three sets of detectors arrays shows a non-steady distribution at values lower than metallic gold Au(0).

Both, positive shift of E_0 and dampening in WL intensity suggest a contraction in electron density surrounding gold nanoparticles in the applied experimental gold conservation material NGG-1b replica. While this means that the gelatin is transferred away from the gold nanoparticles, it also means a successful delivery of both binder and nanogold to the interface layer between gold and iron oxide layers.

Monitoring photoinduced reduction of Au(III) oxide

Monitoring photoinduced reduction of gold in Au(III) oxide was performed through irradiating one position, on a prepared disc of 20 mg of gold oxide in 80 mg cellulose matrix, for ten consequent XANES measurements at Au-L_3 edge collected in fluorescence mode and using same measurement settings. The average experimental XANES measurement time per position was 80 minutes, leading to an accumulative irradiation time of 800 minutes (13.3 hours) at the exact same position. This allows a time dependent XANES study allowing exploring the kinetic impact of synchrotron radiation on gold's chemical speciation. Time-dependant XANES spectra are shown in Figures S6 from which it can be said that gold (III) oxide undergoes photoinduced reduction over time upon irradiation with synchrotron radiation x-rays under room temperature and pressure.

During exposure time the amount of Au^0 in Au_2O_3 changes from 0 wt% to 26 wt% according to the linear combination fit performed in Athena. A kinetic study of photoinduced reduction based on the two end species Au(0) and Au(III) in the form of Au_2O_3 was made possible through a two-component linear combination fit (LCF) of the time-dependant XANES spectra. This is shown in Figure S6c. The concentration of Au(III) oxide species decreases linearly as measurement time increases with a rate constant of 2.36 (linear fit result). On the other hand, the concentration of Au(0) species increases linearly as measurement time increases with the same rate constant 2.36.

Statistical goodness for both linear fitting lines has an R^2 = 0.95257 which indicates a very good fit. So, it is seen that 26 wt% of Au_2O_3 is reduced to metallic gold species in 800 minutes. This means that, if linearly extrapolated, a 100 % conversion would occur after 4000 minutes of continuous irradiation, i.e. 66.7 hours, for the analyte concentration (20 mg).

Stability measurements of NGG were not possible due to the small amount of Gold in it. The impact of photoinduced reduction on gold (III) oxide is to be considered when these compounds are included in LCF as standards. This also applies when they are present in the investigated samples or are formed upon interaction with the interface. At least being aware about this impact is advantageous when designing an experiment with synchrotron radiation and its measuring conditions.

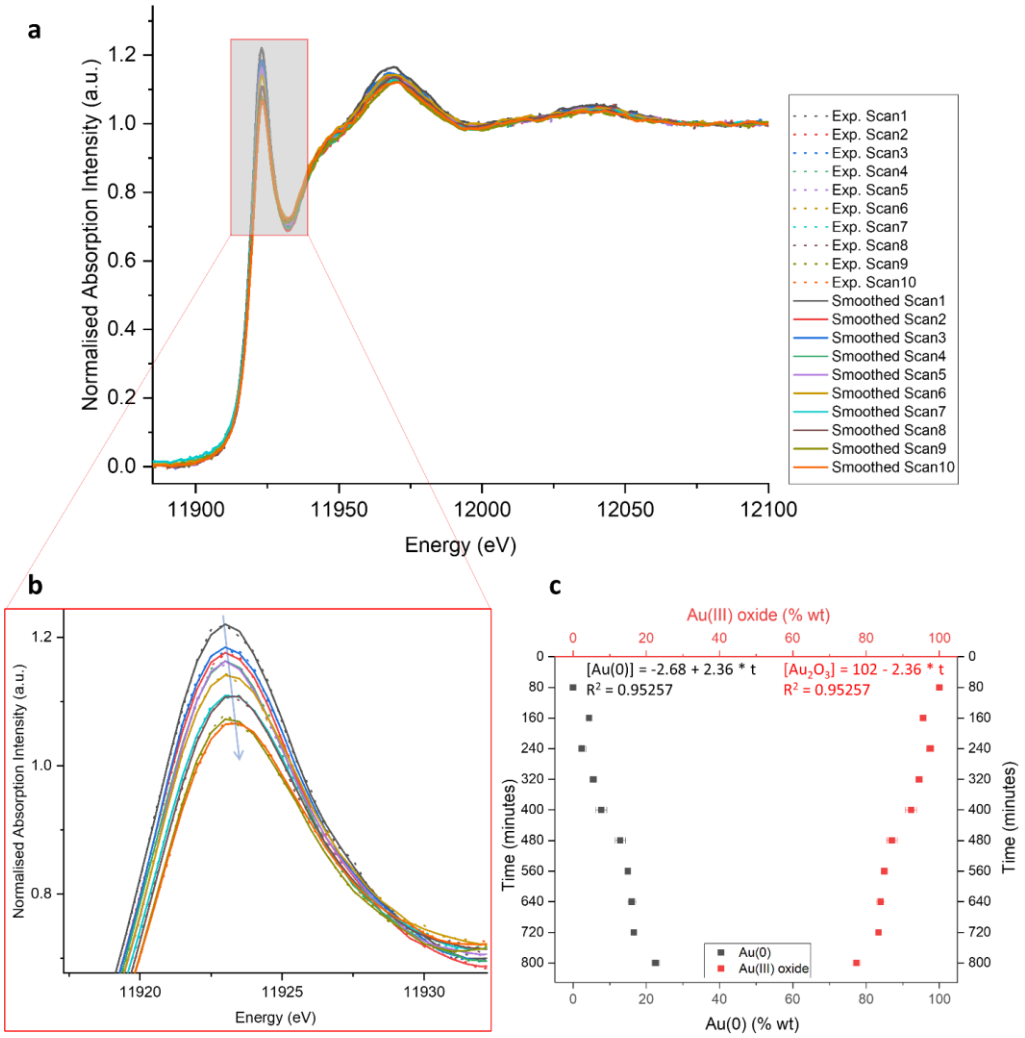

Figure S6: (a) Evolution of Au-L_3 XANES white line spectral dampening and edge shift during time-dependant chemical speciation of Au_2O_3 after (1) 80 min, (2) 160 min, (3) 240 min, (4) 320 min, (5) 400 min, (6) 480 min, (7) 560 min, (8) 640 min, (9) 720 min, and (10) 800 minutes. Experimental data are plotted in dots. Solid lines are smoothed experimental data with 10 points Savitzky Golay function. (b) Magnification of white line region for all spectra. (c) LCF results of Au-L_3 XANES showing variation of Au(0) and Au(III) speciation over time. Linear fitting equations are shown.

Impact of solid angle of detection can be seen at larger angles where a deviation of fluorescence intensity is observed between sets of detectors arrays at the same exit angles.

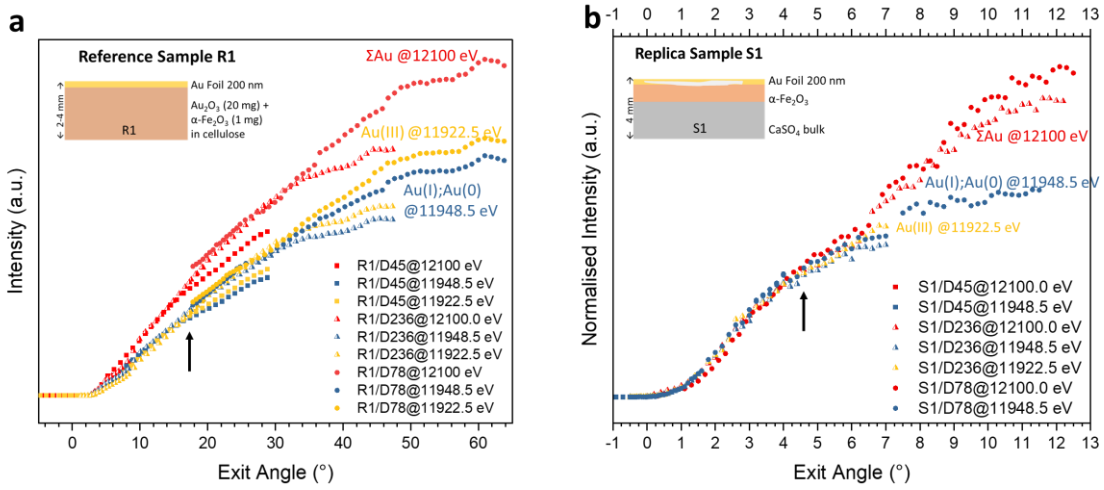

Figure S7: (a) Experimental angular-dependent fluorescence profiles for reference sample R1 at three marker excitation energies for gold [12100.0 eV → Total Au], [11948.5 eV → Au(0,I)], and [11922.5 eV → Au(III)] as recorded at the three sets of detectors arrays. Fluorescence profiles are normalised to incident photon intensity and acquisition time. (b) Angular-dependent fluorescence profiles for the replica sample S1 as read from all three sets of detectors arrays at three marker excitation energies for gold.

Angle-dependent depth distribution of gold species

To depict the depth distribution of gold species based on the angle-dependent measurements an illustration is produced and shown in **Figures S8 and S9**. The illustration connects experimental results of 2D-µXRF elemental maps of a cross section from the replica sample showing major elements and five regions of interest representing (1) Au-layer, (2) NGG1 and NGG2 representing the region directly beneath gold layer, and (3) NGG3 and NGG4 representing regions beneath NGG1 and NGG2, respectively (**Figure S8a, S9a**), AR-XANES spectra at 5° and 45° exit angle of detection (**Figure S8b**), and 2D-µXRF spectra of the five selected regions of interest at gold layer and beneath (**Figure S8c**), and a line scan from sample surface then down across gold layer and NGG beneath (**Figure S9c**). It is to be noted that, spatial resolution of µXRF measurements using Tornado M4 Plus spectrometer[4] is in the range of 18 µm at Au-L_α which is much larger than the nanometre resolution obtained using our AR-XANES method. The NGG regions marked in **Figure S8a and S9a** have a width of 50 µm each.

Due to the non-flat sample surface and irregular penetration depth of NGG, it is difficult to exactly define the depth from which the detected fluorescence signal is generated. The detected fluorescence signal is an accumulative signal generated from all layers reached at the depth correlated to exit angle of detection.

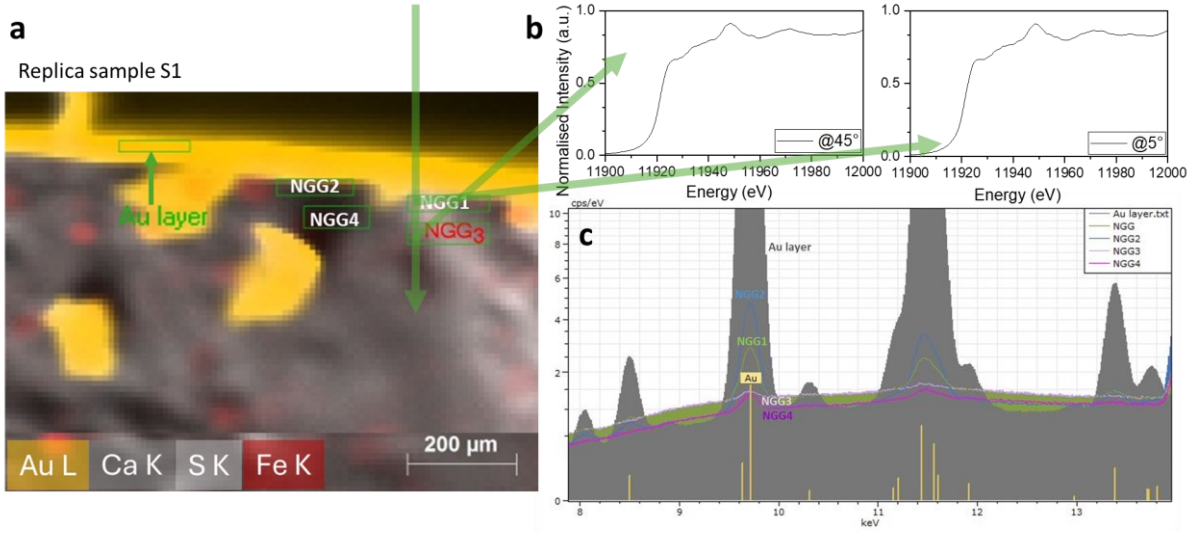

M4 Tornado Plus, 100 Al filter, 50 kV, 1m A, 20 mbar, 10 µm, 1000 x 10 ms

Figure S8: (a) 2D-µXRF elemental maps of a cross section from the replica sample showing the regions of interest, (b) correlated AR-XANES spectra at 5° and 45°. (c) µXRF spectra of the five selected regions of interest representing Au-layer and areas up to 100 µm depth beneath it.

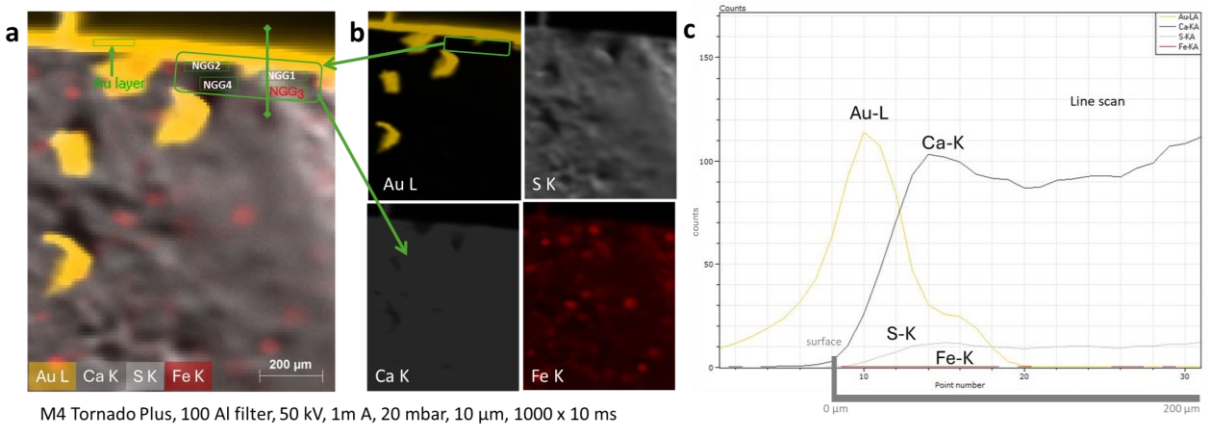

Figure S9: (a) 2D-µXRF elemental maps of a cross section from the replica sample showing the regions of interest and a line scan across the surface and a region of 100 µm below the surface. (b) Individual 2D-µXRF elemental maps of major elements and the further examined region below the surface gold layer. (c) Depth profiles of major elements across the line scan marked in a. Notice the shoulder in Au-L profile indicating a region with lower Au intensity beneath the surface which is likely from NGG.

Surface irregularities of replica samples

Lateral elemental mapping using 2D-µXRF spectroscopy shows irregularities in gold surface layer at the micro-scale (**Figure S10, S11**). This was a major challenge to deal with during the selection of a measurement point for the AR-XANES measurements. Despite the nano-size of gold and its relatively lower concentration in NGG compared to that in the Au-foil, gold signal was detectable using laboratory x-ray tube as excitation source. This indicates that analysing NGG with a synchrotron source will indeed give a well-detected signal.

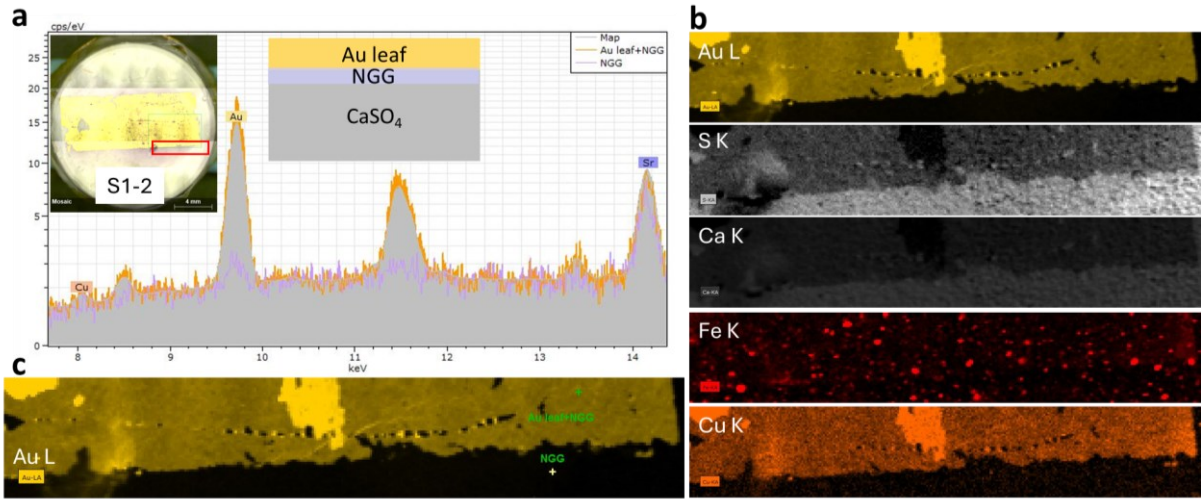

Figure S10: (a) µXRF spectra of two selected regions of interest shown in c representing Au-leaf with NGG beneath (orange spectrum), and NGG alone (purple spectrum). The map µXRF spectrum of the whole region marked in a red rectangle in the inset is also shown. A schematic illustration of layers structure of this replica sample is shown in the inset too. (b) Individual 2D-µXRF elemental maps of major elements using M4 Tornado Plus, 100 Al filter, 50 keV, 1 mA, 20 mm, 20 mbar. (c) Au-L elemental map marking both regions of interest (point analysis) of which spectra were compared in a.

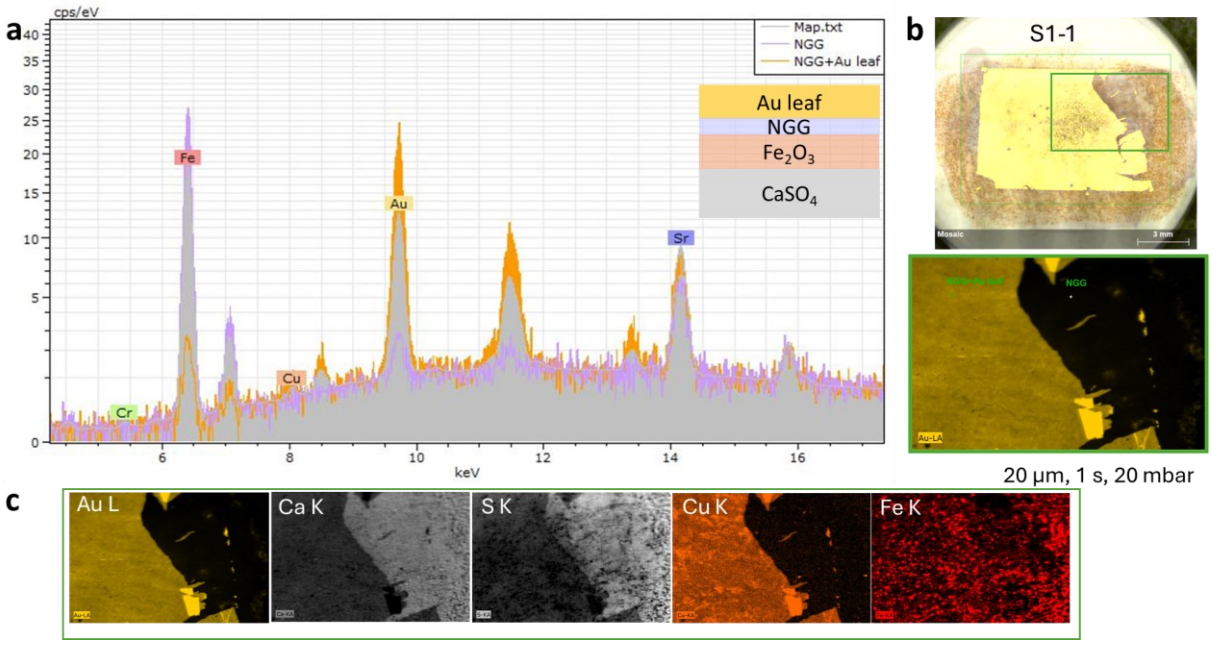

Figure S11: (a) µXRF spectra of two selected regions of interest shown in b representing Au-leaf with NGG beneath (orange spectrum), and NGG alone (purple spectrum). The map µXRF spectrum of the whole region marked in a green rectangle in b is also shown. A schematic illustration of layers structure of this replica sample is shown in the inset. (b) (top) Image of the analysed sample with a green rectangle showing the mapped region. (bottom) Au-L elemental map marking both regions of interest (point analysis) of which spectra were compared in a. (c) Individual 2D-µXRF elemental maps of major elements using M4 Tornado Plus, 100 Al filter, 50 keV, 1 mA, 20 mm, 20 mbar.

Surface irregularities of reference sample

Lateral elemental mapping using 2D-µXRF spectroscopy shows irregularities in gold surface layer at the micro-scale (**Figure S12**). This was indeed a major challenge to deal with during the selection of a measurement point for the AR-XANES measurements.

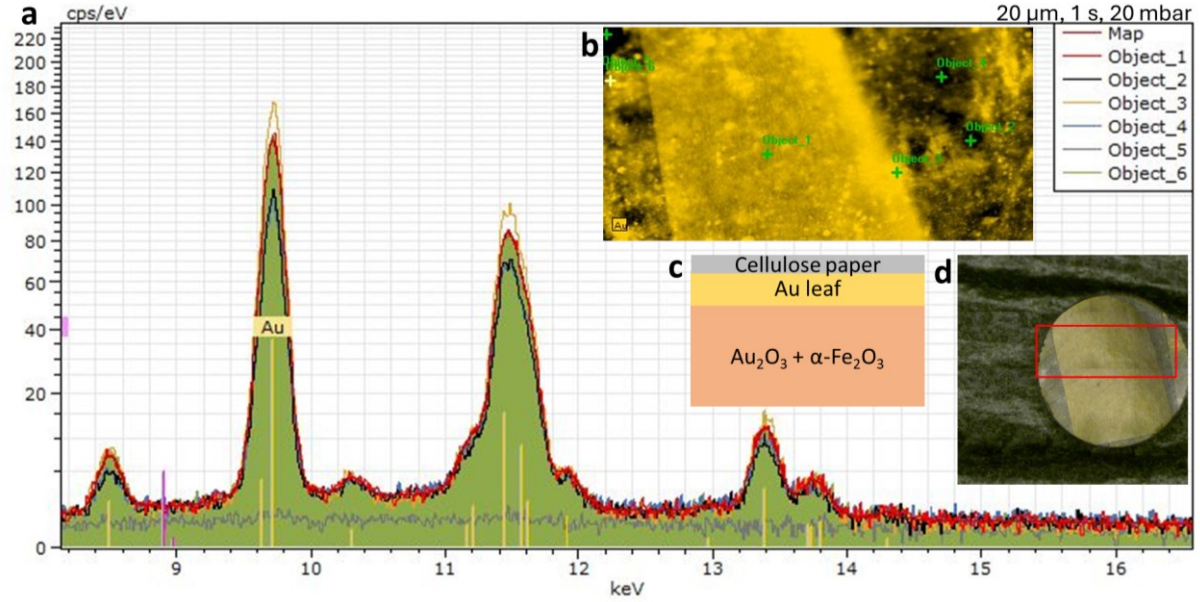

Figure S12: (a) µXRF spectra of the five selected regions of interest representing Au-layer. (b) Au-L elemental map as analysed by 2D-µXRF spectroscopy and regions of interest measured as points with their spectra shown in a. (c) Schematic illustration of layers structure of the reference sample R1. (d) Microscopic image of the sample marking the measured lateral map (red rectangle) of which spectrum is shown as map spectrum in a.

Bibliography

1. Wedekind, W. Weathering and conservation of monuments constructed from tuff and sandstone in different environmental conditions. Case studies from Mexico, germany, Jordan and Cambodia. (2016).

2. Wedekind, W. & Fischer, H. Evaluation of Desalination and Restoration methods applied in Petra (Jordan). in *SWBSS 2017 Fourth International Conference on Salt Weathering of Buildings and Stone Sculptures Verlag der Fachhochschule Potsdam* pp190-199 (2017).

3. Zizak, I. mySpot: a versatile microfocussing station for scanning methods at BESSY II. *J. large-scale Res. Facil. JLSRF* **2**, 1–10 (2016).

4. Förste, F. *et al.* Quantification routines for full 3D elemental distributions of homogeneous and layered samples obtained with laboratory confocal micro XRF spectrometers. *J. Anal. At. Spectrom.* **37**, 1687–1695 (2022).